



Aerodynamics of a Trapped Vortex Combustor: A Comparative Assessment of RANS Based CFD Models

Open
Access

Hesham Khalil^{1,*}, Khalid Saqr², Yehia Eldrainy¹, Walid Abdelghaffar¹

¹ Mechanical Engineering Department, Faculty of Engineering, Alexandria University, Alexandria, Egypt

² Mechanical Engineering Department, Arab Academy for Science, Technology and Maritime Transport, Alexandria, Egypt

ARTICLE INFO

ABSTRACT

Article history:

Received 5 February 2018

Received in revised form 21 February 2018

Accepted 22 February 2018

Available online 7 March 2018

Trapped vortex combustion, TVC, has shown promising results in terms of wide stability range and low pressure drop. However, previous experimental and numerical studies, which were limited to DNS, have provided only global performance assessments. Also, high computational cost limitations of DNS motivated the need for evaluating other lower cost turbulent models. Consequently, three RANS turbulence models were assessed in the present work; RKE, SST-KW, and RSM, using 2D numerical computations. In addition, the effect of inlet flow Re on cavity flow physics and stability was explored for more detailed physical insight. Ansys Fluent 12 has been used in the computations with the steady state compressible pressure based solver. RSM was found to have the least prediction error percentage against experimental data with maximum value of 12.1% for all cases studied compared with 23.9 % demonstrated by the SST-KW which was the least accurate model. Increasing inlet flow Re by order of magnitude had no apparent effect on the main flow structure for the same cavity size. However, the 300 % Re increase from 9229 to 27687 has led to 10 times increase in turbulence levels and 3 times increase in recirculation zone strength which confirms the high stability range of these combustors. Finally, multiple vortex structures, either behind the forebody for smaller cavity sizes of $H/D_f < 0.6$ or behind the afterbody for larger cavity sizes $H/D_f > 1$, were noticed to be the main reason behind increased pressure drop from 0.8 to 1.1%. This study was conducted as a ground base for future TVC analysis.

Keywords:

Trapped vortex combustors, cavity flows, turbulent modelling, CFD, drag reduction

Copyright © 2018 PENERBIT AKADEMIA BARU - All rights reserved

1. Introduction

Flow over cavities is one of the classical problems that have been studied extensively by the aerodynamic community through the past decades while trying to enhance pressure recovery and reduce drag [1-5]. Little and Whipkey [3] experimentally investigated the effect of adding an

* Corresponding author.

E-mail address: hekhalil@alexu.edu.eg (Hesham Khalil)

additional disk downstream a bluff body using a system of two tandem disks connected by a central spindle. Using several geometries, they concluded that for a minimum drag to be reached, the cavity between the two disks has to be properly sized. They developed relations between both the cavity length (H), and the afterbody diameter (D_{aft}) and the forebody diameter (D_f) to achieve this purpose. It was found that for $D_{aft} / D_f < 1$ (nearly 0.75), minimum drag can be achieved using a value of H/D_f around 0.6.

Following these efforts, Hsu *et al.* [4] investigated the potential of using cavity trapped vortices in combustion as a new way of flame stabilization using a similar geometry. They developed a 'Trapped vortex combustor' where, beside the main stream air, primary air and fuel were injected directly into the cavity to ensure continuous combustion and also to better control the local equivalence ratio. The novel combustor demonstrated very low pressure drop (order of magnitude lower than state of the art lean premixed combustors), wide stability range and high combustion efficiencies. They suggested that the wide stability range is mainly due to the isolation of the combustion reaction zone inside the cavity away from upstream flow variations. Motivated by these results, and due to its showing potential, several studies were conducted to investigate the application of trapped vortex combustors in gas turbines either alone [6-15], or combined with other combustion strategies [16].

In addition, Katta and Roquemore [17, 18] conducted numerical computations to study flow dynamics in different cavities geometries under both non-reacting and reacting conditions. Both direct numerical solutions (DNS) and unsteady Reynolds averaged models (URANS) were used in their work to predict drag coefficient with reasonable agreement. They suggested an initial decrease in drag coefficient with the increase of cavity length till a minimum value is reached. Following this minimum value the drag starts to increase for larger cavities. They also concluded that drag force is governed by large scale fluid structures with minimal effect of small turbulence length scales. Finally, using DNS, they related high drag of cavities with $H/D_f < 0.6$ to the multiple vortex structure showed inside the cavity. They demonstrated one dominant stable vortex inside the cavity and another one downstream the afterbody for cavities of H/D_f close to 0.6 which was the main reason behind minimum drag at this condition. For larger cavities the same single vortex existed inside the cavity while multiple vortex structure was shown behind the afterbody.

Transient simulations showed that the cavity vortex was not stable and was usually rotating around the cavity center. DNS were able to correctly capture the flow physics compared with the experiments unlike the URANS standard k-epsilon model used. However, DNS, although more accurate, remains constrained by its high computational cost which limits its use to one and two-dimensional geometries in most cases [19]. These results were confirmed by other numerical works [20].

As a result, the present work aims at assessing the performance of more advanced URANS turbulence models in terms of pressure drop and flow physics predictions within the scope of cavity trapped vortices. It also aims at gaining more physical insight of the flow physics inside the cavity to provide a suitable ground for its further use in combustion. The numerical methods used in the present study are first re-visited followed by a demonstration of the computational framework used. Subsequently, pressure drop computations using different turbulent models are presented. After that, cavity flow structure is investigated in details at various cavity sizes and Reynolds numbers. Finally, major findings and conclusions of this study are summarized.

2. Methodology

2.1 Reynolds Averaged Navier Stokes Approach

The unsteady Reynolds averaged continuity and momentum Navier Stokes equations in the compressible form are given as [21]:

$$\frac{\partial \rho}{\partial t} + \frac{\partial}{\partial x_i} (\rho u_i) = 0. \quad (1)$$

$$\frac{\partial}{\partial t} (\rho u_i) + \frac{\partial}{\partial x_j} (\rho u_i u_j) = -\frac{\partial p}{\partial x_i} + \frac{\partial}{\partial x_j} \left[\mu \left(\frac{\partial u_i}{\partial x_j} + \frac{\partial u_j}{\partial x_i} - \frac{2}{3} \delta_{ij} \frac{\partial u_l}{\partial x_l} \right) \right] + \frac{\partial}{\partial x_j} (-\rho u_i' u_j'). \quad (2)$$

Where ρ is the density of the fluid, t is the time, and u_i is a mean component of velocity in the direction x_i , p is the pressure, μ is the dynamic viscosity, and u_i' is a fluctuating component of velocity. Repeated indices indicate summation from one to two. The term $-\rho u_i' u_j'$ expresses the Reynolds stresses which are modeled using Boussinesq hypothesis [21, 22] which relates the Reynolds stresses to the mean velocity gradients:

$$-\rho u_i' u_j' = \mu_t \left(\frac{\partial u_i}{\partial x_j} + \frac{\partial u_j}{\partial x_i} \right) - \frac{2}{3} \left(\rho k + \mu_t \frac{\partial u_k}{\partial x_k} \right) \delta_{ij} \quad (3)$$

Where k is the turbulent kinetic energy, as defined by $k = \frac{1}{2} \overline{u_i' u_i'}$, and δ_{ij} is the Kroneker delta. An advantage of the Boussinesq approach is the relatively low computational cost associated with the computation of the turbulent viscosity μ_t . A disadvantage is that it assumes μ_t is an isotropic scalar quantity, which is not always the case. The Realizable k -epsilon model is an example of two-equation models that use the Boussinesq hypothesis.

2.1.1 Realizable k - ϵ model (RKE)

The term “realizable” means that the model satisfies certain mathematical constraints on the Reynolds stresses, consistent with the physics of turbulent flows. It is based on the work of Shih et al. [23] and differs from other k -epsilon models in two ways:

- The realizable k -epsilon model contains a new formulation for the turbulent viscosity.
- A new transport equation for the dissipation rate, ϵ , has been derived from an exact equation for the transport of the mean-square vorticity fluctuation.

The transport equations for both k and ϵ are shown below [23]:

$$\frac{\partial}{\partial t} (\rho k) + \frac{\partial}{\partial x_j} (\rho k u_j) = \frac{\partial}{\partial x_j} \left[\left(\mu + \frac{\mu_t}{\sigma_k} \right) \frac{\partial k}{\partial x_j} \right] + G_k + G_b - \rho \epsilon - Y_M + S_k \quad (4)$$

$$\frac{\partial}{\partial t} (\rho \epsilon) + \frac{\partial}{\partial x_j} (\rho \epsilon u_j) = \frac{\partial}{\partial x_j} \left[\left(\mu + \frac{\mu_t}{\sigma_\epsilon} \right) \frac{\partial \epsilon}{\partial x_j} \right] + \rho C_1 S_\epsilon - \rho C_2 \frac{\epsilon^2}{k + \sqrt{U \epsilon}} + C_{1\epsilon} \frac{\epsilon}{k} C_{3\epsilon} C_b + S_\epsilon \quad (5)$$

where

$$C_1 = \max \left[0.43, \frac{\eta}{\eta + 5} \right], \quad \eta = S \frac{k}{\epsilon}, \quad S = \sqrt{2 S_{ij} S_{ij}}$$

G_k represents the generation of turbulence kinetic energy due to the mean velocity gradients, G_b is the generation of turbulence kinetic energy due to buoyancy, and Y_M represents the contribution of

the fluctuating dilatation in compressible turbulence to the overall dissipation rate. C_2 and $C_{1\epsilon}$ are constants. σ_k and σ_ϵ are the turbulent Prandtl numbers for k and ϵ , respectively. S_k and S_ϵ are any other defined source terms.

2.1.2 Shear stress transport k -omega model (SST $k - \omega$)

The shear stress transport k -omega model was developed by Menter [24] to effectively blend the robust and accurate formulation of the k -omega model in the near-wall region with the free-stream independence of the k -epsilon model in the far field. To achieve this, the k -epsilon model is converted into a k -omega formulation. The SST k -omega model is similar to the standard k -omega model, but includes the following refinements:

- The standard k -omega model and the transformed k -epsilon model are both multiplied by a blending function and both models are added together. The blending function is designed to be one in the near-wall region, which activates the standard k -omega model, and zero away from the surface, which activates the transformed k -epsilon model.
- The SST model incorporates a damped cross-diffusion derivative term in the omega equation.
- The definition of the turbulent viscosity is modified to account for the transport of the turbulent shear stress.
- The modeling constants are different.

The transport equations for both k and omega ω are shown below [24] :

$$\frac{\partial}{\partial t}(\rho k) + \frac{\partial}{\partial x_i}(\rho k u_i) = \frac{\partial}{\partial x_j} \left(\Gamma_k \frac{\partial k}{\partial x_j} \right) + G_k - Y_k + S_k \quad (6)$$

$$\frac{\partial}{\partial t}(\rho \omega) + \frac{\partial}{\partial x_i}(\rho \omega u_i) = \frac{\partial}{\partial x_j} \left(\Gamma_\omega \frac{\partial \omega}{\partial x_j} \right) + G_\omega - Y_\omega + D_\omega + S_\omega \quad (7)$$

Where, G_ω represents the generation of turbulence specific dissipation rate, Γ_k and Γ_ω represent the effective diffusivity of k and ω , respectively, Y_k and Y_ω represent the dissipation of k and ω due to turbulence, D_ω represents the cross-diffusion term, S_k and S_ω are any other-defined source terms.

2.1.3 Reynolds Stress Model (RSM)

Founded by Launder *et al.* [25], Reynolds stress model does not follow Boussinesq hypothesis and takes account for anisotropic turbulence by solving Reynolds stresses using a developed transport equation for each of them along with a transport equation for the dissipation rate. That means additional five transport equations to be solved for 2D problems and seven equations for 3D problems which makes the model computationally more expensive than the two-equation models. However, it usually gives more accurate predictions when it comes to problems involving swirling flows, flow rotations or rapid changes in strain rate.

2.2 Computational Domain

Two domains have been investigated in the present study. The first one is a complete 3D domain shown in Fig. (1) which will be used to validate the 2D axisymmetric assumption, and the another one shown in Fig. (2) is the 2D section for the upper half of the combustor which will be

used in all the subsequent computations. The experimental findings of Hsu *et al.* [4] will be used for validation of our numerical scheme results and assessment of turbulent models.

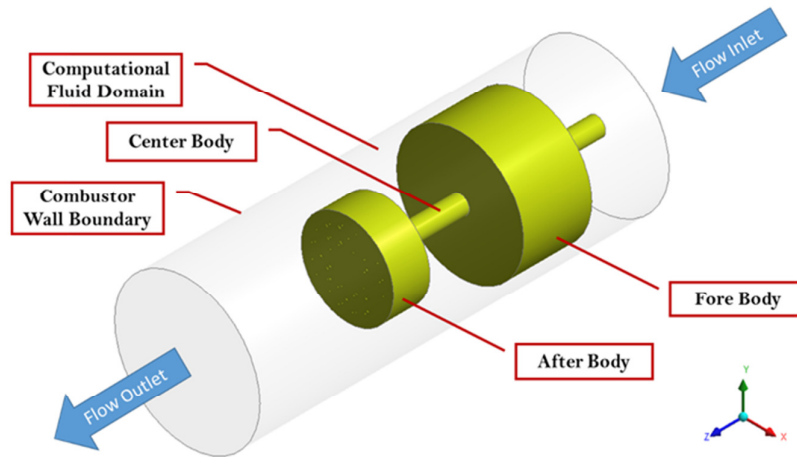


Fig. 1. 3D schematic of the computational domain used in present work

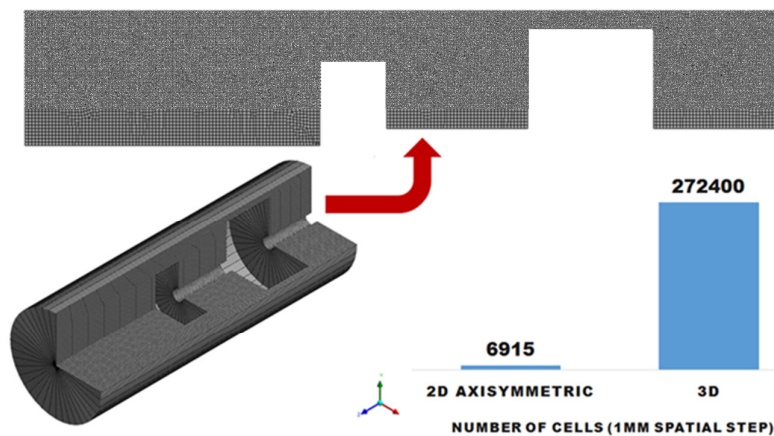


Fig. 2. 3D and 2D Computational grids used in present work

2.3 Numerical Set-Up and Boundary Conditions

In this study, simulations were performed using the ANSYS Fluent 12.1 CFD software. The prescribed compressible form of governing equations has been solved by means of steady state solver using a pressure based finite volume methodology. PRESTO was used to solve the pressure correction equation while ideal gas law has been used for density. A second order upwind scheme was used for the momentum, turbulence kinetic energy, turbulence dissipation rate, and the energy equations. Convergence criteria were set to four orders of magnitude reduction for continuity equation and fifth order of magnitude for all other equations. All simulations have been run on a desktop computer with an Intel core i7 CPU (3.2 GHz, 16 GB RAM).

2.3.1 Boundary conditions

Table 1 shows the operational cases included in the present work. Mass flow inlet was applied at the inlet boundary, while pressure outlet was set at the exit. To determine mass flow inlet at various cases included in table (1), preliminary numerical computations have been conducted using the experimental data of pressure drop across the combustor in [4] at various annular air velocities studied. Computed mass flow rates at various Reynolds numbers studies are shown in table (2). Adiabatic and no-slip boundary conditions have been used for all combustor walls.

Table 1
Cases under investigation in present work

D_f (mm)	D_{aft} (mm)	H/ D_f	Annular Velocity (m/s)	Annulus Reynolds Number
70	50.8	0.2, 0.6, 1, 1.4, 1.8	42	27687
70	50.8	0.2, 0.6, 1, 1.4, 1.8	28	18458
70	50.8	0.2, 0.6, 1, 1.4, 1.8	14	9229

Mass flow inlet was applied at the inlet boundary, while pressure outlet was set at the exit. To determine mass flow inlet at various cases included in table (1), preliminary numerical computations have been conducted using the experimental data of pressure drop across the combustor in Hsu *et al.*, [4] at various annular air velocities studied. Computed mass flow rates at various Reynolds numbers studies are shown in table (2). Adiabatic and no-slip boundary conditions have been used for all combustor walls.

Table 2
Mass flow inlet at various Reynolds numbers studied

Annular Velocity (m/s)	Annulus Reynolds Number	Computed Mass Flow Inlet (g/s)
42	27687	47.6
28	18458	33.6
14	9229	17.1

3. Results and Discussion

In this section, both validation of numerical assumptions and grid independent study will be first demonstrated. Then, pressure drop predictions will be made at various cavity length and main stream Reynolds number. Different turbulent models performance will be assessed as well against experimental data. Finally, the effect of both cavity length and main stream Reynolds number on flow structure and strain rate will be investigated.

3.1 Validation of 2D Axisymmetric Assumption against 3D Complete Domain

The two dimensional axisymmetric assumption of the combustor was investigated against the 3D complete solution using a case of 59 g/s inlet mass flow rate and a grid resolution of 6900 cells for the 2D section and 272400 cells for the 3D section. Fig. (2) shows the 2D and 3D sections and the grid used. The main target of this study is to get confidence about the ability of the 2D domain to capture the same physics of the flow as the complete domain. Fig. (3) shows the locations at which comparisons were made.

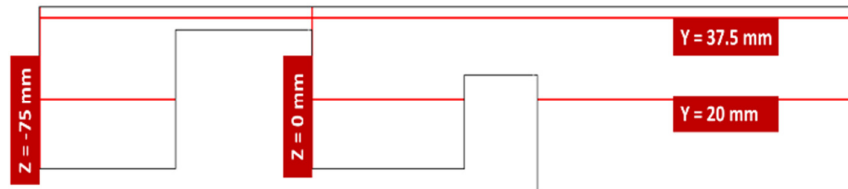
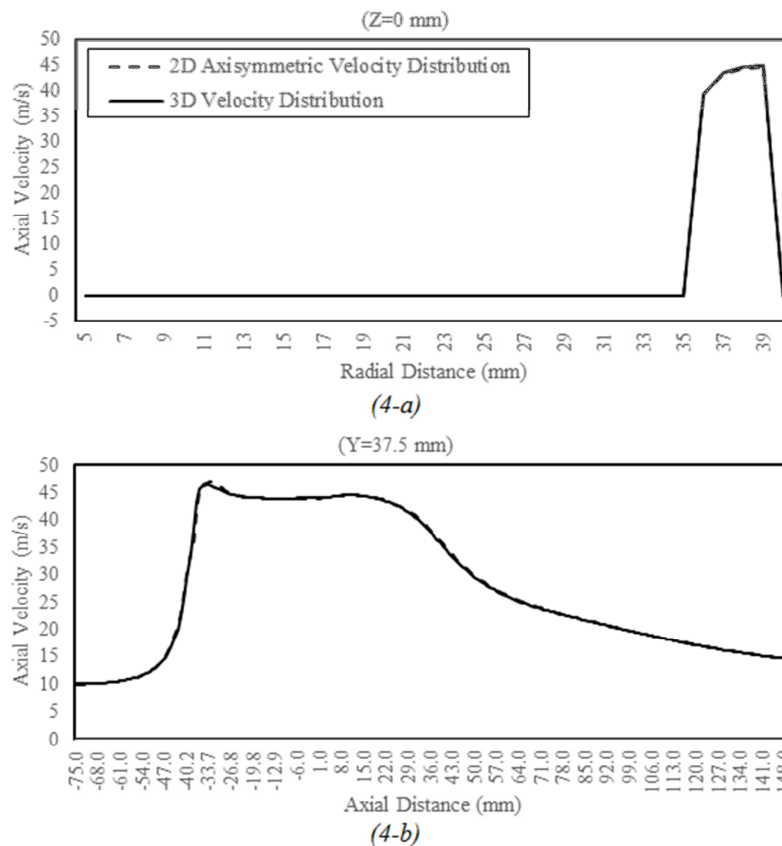


Fig. 3. Locations of velocity and pressure distributions for 2D-3D comparisons

Figure (4 a-f) demonstrates comparisons of both axial velocity and pressure distributions along the locations mentioned above for both cases; 2D axisymmetric and 3D domains. From Fig. (4a-f) it can be concluded that there is a perfect agreement between axial velocity and pressure computations using 2D axisymmetric geometry and 3D complete domain at all locations studied which suggests the validity to use the 2D axisymmetric domain in the following computations with confidence.



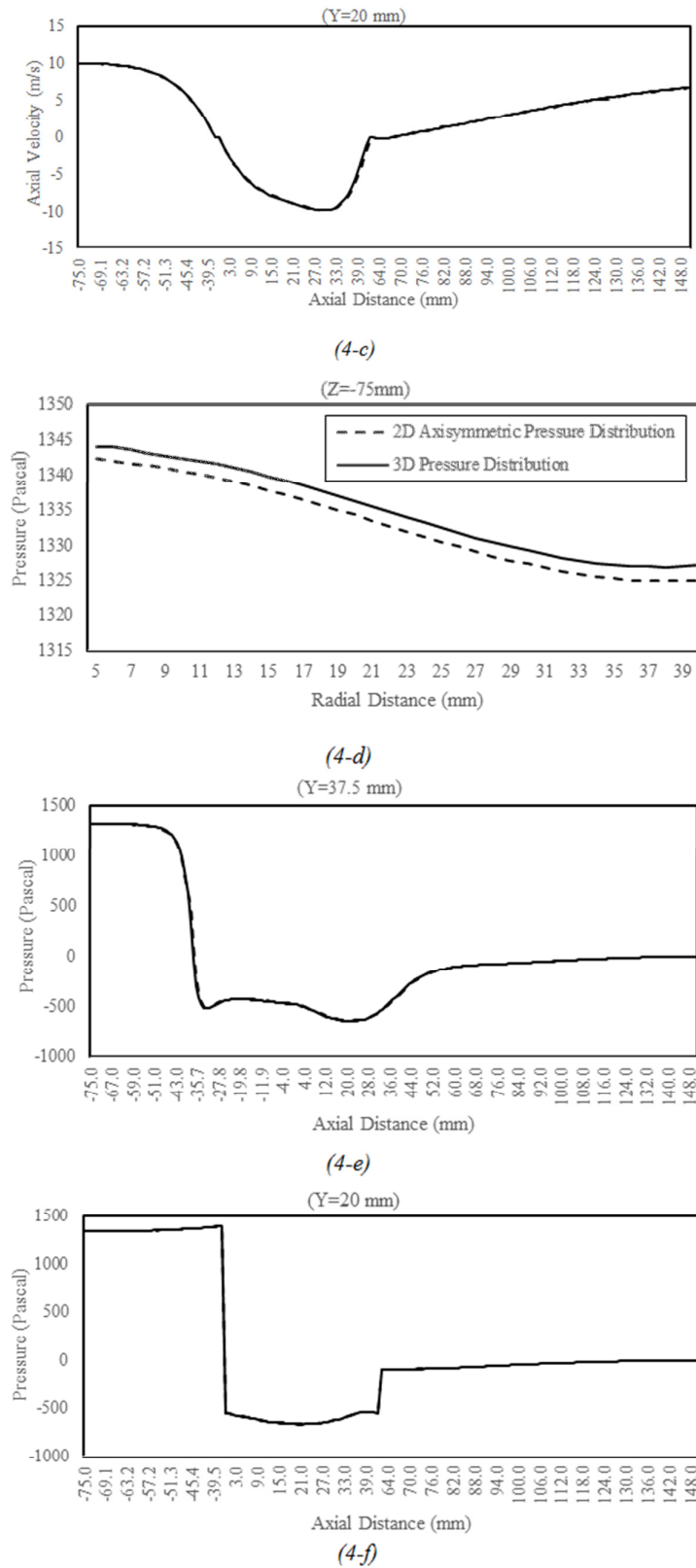


Fig. 4. Axial velocity and pressure distribution comparisons for 2D axisymmetric vs. 3D computations

3.2 Grid Independent Study

Before going through pressure drop and flow physics predictions, three grid resolutions were tested to determine a grid independent solution. Fig. (5) demonstrates the three grids under investigation against the grid spacing in each case. It's noteworthy to mention that wall refinement has been applied at all near wall regions.

The first case in table (1) ($Re=27687$) was used in the grid independent computations as it is the highest Reynolds number investigated in the present study. A Cavity length to forebody diameter ratio (H/D_f) of 0.6 cavity was chosen. Realizable K-epsilon model was used in all computations. Fig. (6a-c) demonstrates the results of the grid independent computations. From these figures it is noted that both grids 30000 and 100000 lead to similar solutions although they are order of magnitude apart. The coarse grid (8800 cells) has slightly under predicted the axial velocity values at annular inlet at some locations, see Fig. (6-a). It has also over predicted the static pressure at the inlet of the combustor as seen in Fig. (6-c). For these reasons, it seems possible to use the medium grid (30000 cells) in all the following computations.

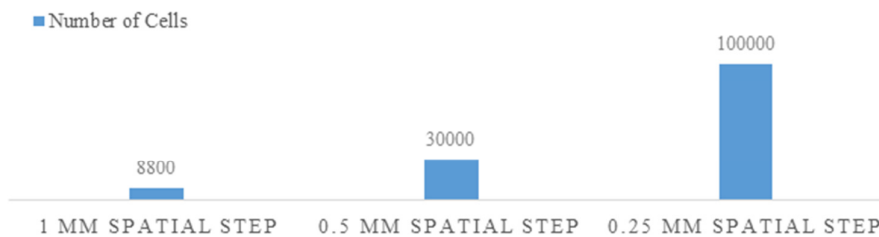
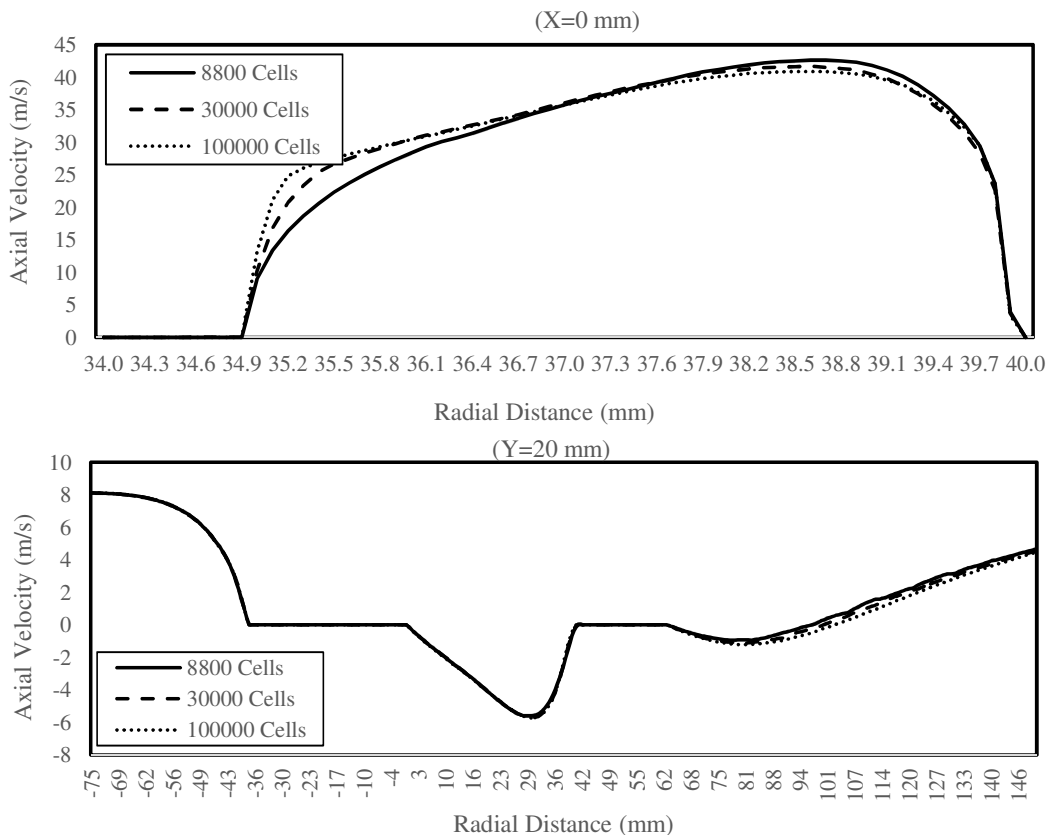


Fig. 5. Grid resolutions used vs. grid spacing



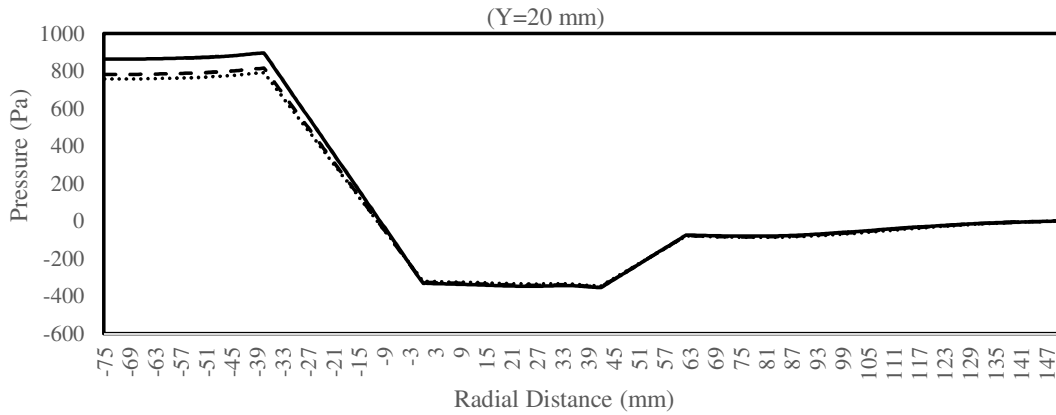
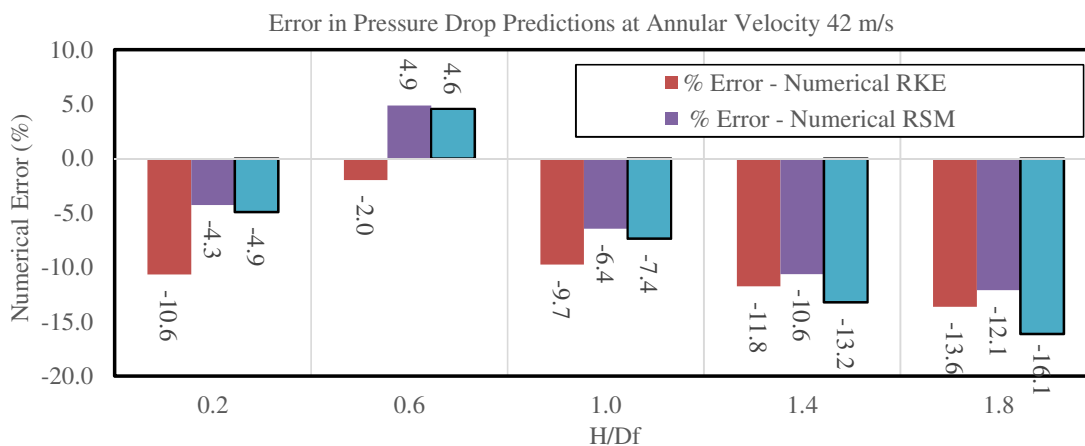
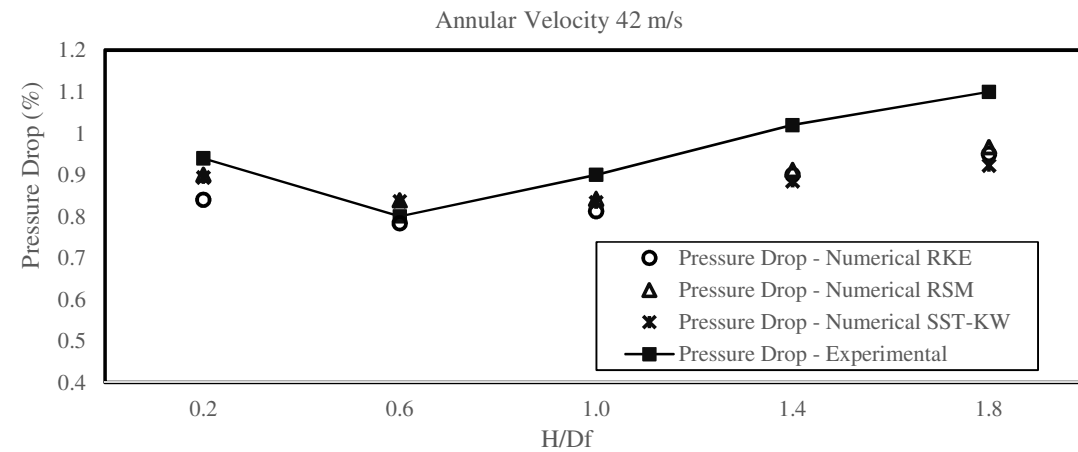


Fig. 6. Velocity and pressure distributions at different grids and combustor locations

3.3 Pressure Drop Predictions and Turbulence Models Assessment

Pressure drop across the combustor has been estimated at different Reynolds numbers and cavity sizes. Three turbulent models; RKE, SST-KW, and RSM, have been used in the present computations to assess their performance in terms of their ability to predict the pressure drop correctly. Fig. (7 a-f) demonstrates these numerical computations. Experimental data from [4] have been used for comparison and validation.



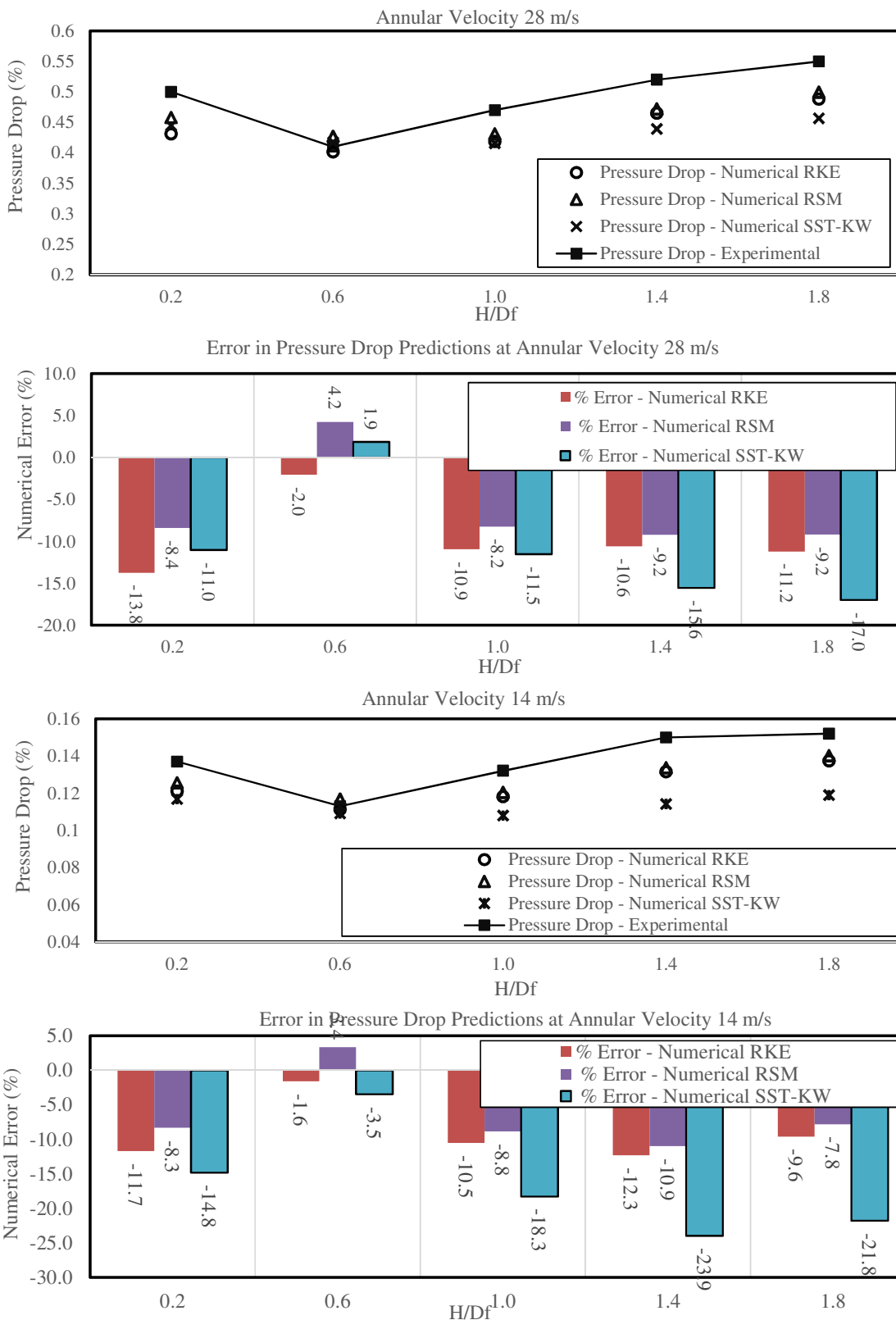


Fig.7. Pressure drop computations and error estimation for various Reynolds numbers, cavity sizes and turbulence models

It can be noted from Fig. (7-a, 7-c, 7-e) that minimum pressure drop occurs at certain cavity length regardless the main stream conditions (Reynolds number). This cavity length corresponds to H/D_f ratio of 0.6 which is consistent with the experimental data of Hsu et al. [4] and also the results of Little and Whipkey [3]. For cavity sizes smaller or larger, pressure drop starts to increase. It is also noted from the mentioned figures that variation of pressure drop with cavity length becomes more noticeable as main stream Reynolds number increases which is also consistent with the results of Hsu *et al.* [4]. It is noteworthy to mention that the highest pressure drop encountered through the present cases is 1.1 % which is considerably lower than values encountered in the state of the art lean premixed combustors. This offers a great potential to use trapped vortex in gas turbine combustion application.

Figs. (7-b, 7-d, 7-f) show the percentage of prediction error for each of the turbulence models used for various cases compared with the experimental findings. It can be noted that the Reynolds stress model has the most accurate predictions over the other two models. It has the least prediction error percentage against experimental data with maximum value of 12.1% for all cases studied compared with 23.9 % demonstrated by the SST-KW which was the least accurate model. This is expected as it accounts for the turbulence anisotropy which is apparent in this type of problems that involve both rotating flow and high strain rates. However, all turbulent models were able to capture the pressure drop variation with cavity size in a correct qualitative manner. It is also noteworthy to say that SST-KW sometimes gives better results compared with RKE [26, 27].

3.4 The Effect of Re and Cavity Width on Flow Structure

Numerical computations using the RSM model have been conducted to investigate the effect of both cavity size and main stream Reynolds number on the flow structure of the trapped vortex combustor. Fig.8 (a-f) shows the steady state flow structure at different Reynolds numbers for a cavity size of $H/D_f=0.2$. Three Reynolds numbers have been investigated; 27687 (Fig. 8(a, b)), 18458 (Fig. 8(c, d)), and 9229 (Fig. 8(d, e)) which correspond to annular air velocity of 42, 28, and 14 m/s respectively. Velocity vectors and stream lines represented demonstrate multiple vortex structures inside the small cavity as shown in Fig. (8-a, b). This multiple vortex structure contain 3 vortices; two upper vortices and a corner one. The two upper vortices appear to rotate in opposite directions relative to each other; clockwise for the upper one and counterclockwise for the lower one, which agrees well with Katta and Roquemore [17] direct numerical solutions for this cavity size. This supports the confidence about the ability of RSM model to correctly capture the flow physics for cavity flows. On the other side, a single large vortex was noted behind the afterbody. The increased pressure drop at this cavity size is apparently because of this multiple vortex structure inside the cavity.

Comparing Fig. 8(a, b) with 8(c, d) and 8(e, f), similar flow structure was noticed regardless the Reynolds number. As a result, Reynolds number is noticed to have apparently no effect on the flow structure for the same cavity size. Also, it can be noted from Figs. (8-b, d, f) that turbulent kinetic energy is very low which is apparently due to the dominant wall effect despite the multiple vortical structures noticed inside the cavity.

Flow structure at cavity size of $H/D_f=0.6$ is shown in Fig. 9(a-f). The flow was noticed to be divided into two large single vortices; one inside the cavity and another behind the afterbody. Both vortices rotate in clockwise direction following the flow main stream. Again the results are consistent with the direct numerical solutions of Katta and Roquemore [17]. These stable vortices are apparently the reason of the minimum pressure drop at this cavity size. Similar to the previous geometry, Reynolds number is noticed to have no apparent effect on the flow structure. However, turbulence levels increased 10 times as noticed in Figs. (9-b), (9-d), and (9-f).

Similar results were achieved at cavity size of $H/D_f=1$ as seen from Fig. 10(a-f). However, the cavity vortex center appears to move downstream the combustor following the motion of the afterbody. Also, turbulence levels increased inside the cavity as noticed from Figs. (10-b), (10-d), and (10-f). This could result in better mixing characteristics and enhanced combustion stability if a trapped vortex combustor cavity was selected in this range (0.6 to 1).

For larger cavity sizes; $H/D_f > 1$, multiple vortex structure appear to exist behind the afterbody. This multiple vortex structure behind the afterbody can provide a possible explanation for the increased pressure drop with cavity size. Fig. 11(a-f) and 12(a-f) demonstrates the flow structure for cavity sizes $H/D_f > 1.4$, and $H/D_f > 1.8$ respectively. Similar to previous smaller sizes, Reynolds number has no apparent effect on flow structure except the increased turbulence levels. This could be an advantage considering combustion as it implies that the flow field, hence the linked combustion characteristics, are completely isolated from upstream conditions.

3.5 The Effect of Re and Cavity Width on Cavity Recirculation Zone

Fig. 13 to 17 show the axial velocity distribution along the cavity centerline for different cavity sizes and Reynolds numbers. Increasing inlet flow Re by 300 % from 9229 to 27687, hence it can be considered as one order of magnitude increase, leads to 3 times increase in the recirculation zone strength. It can also be noted that the cavity recirculation zone strength increases with the increase of cavity length while the vortex is squeezed more toward the center body. Finally, increasing cavity size leads to an increase in the cavity recirculation zone strength for the same main stream Reynolds number, hence it has the same effect as increasing Reynolds number for the same cavity size.

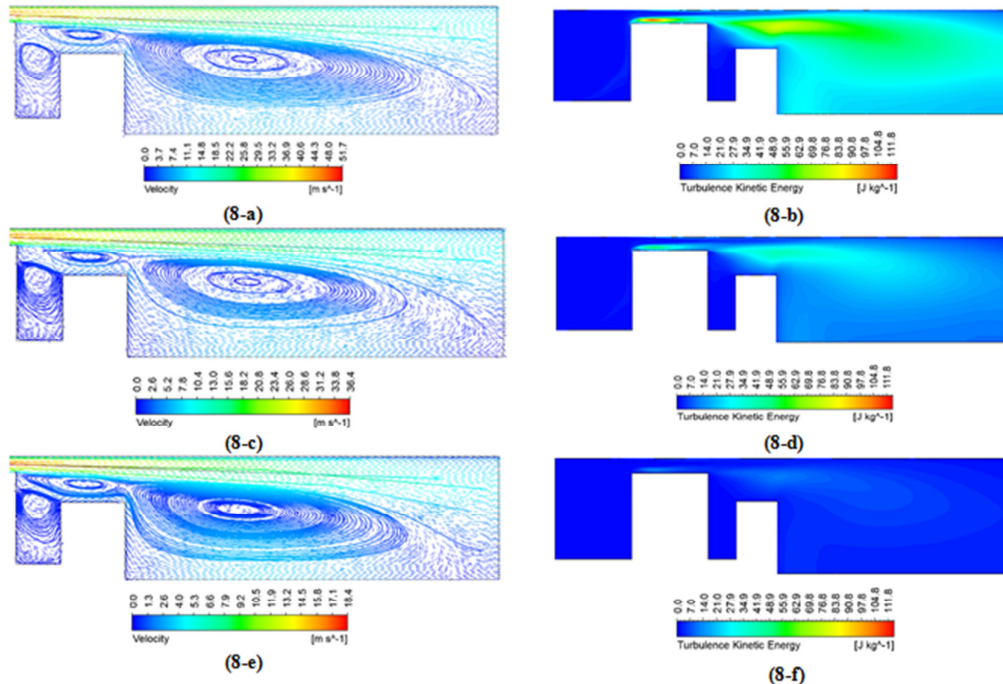


Fig. 8. Cavity flow structure at (8-a, b) $Re=27687$, (8-c, d) $Re=18458$, and (8-e, f) $Re=9229$ for $H/D_f = 0.2$

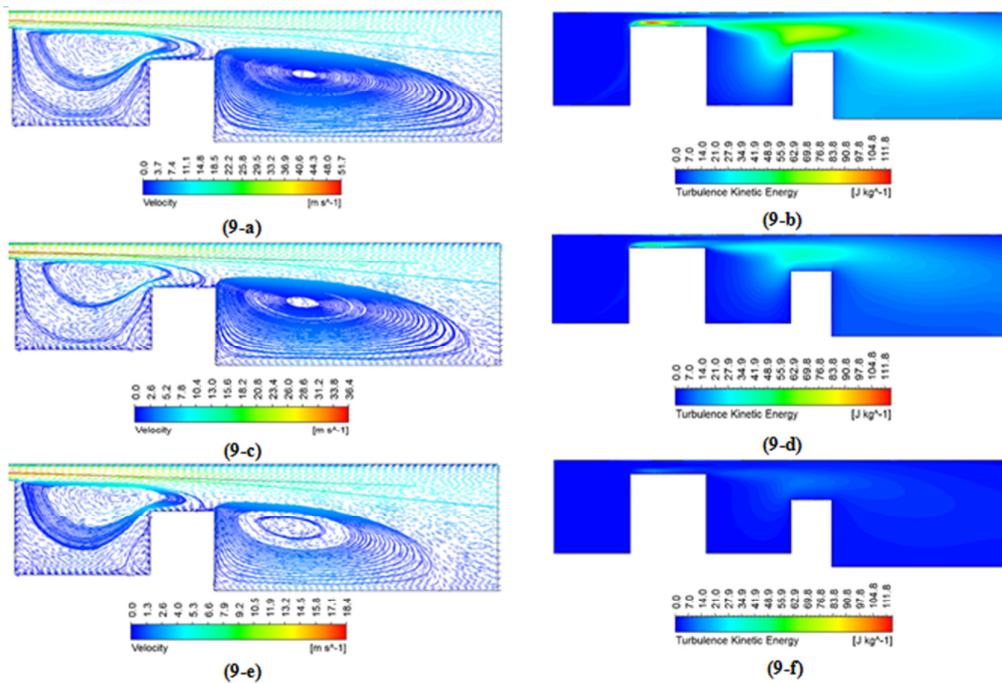


Fig. 9. Cavity flow structure at (9-a, b) $Re=27687$, (9-c, d) $Re=18458$, and (9-e, f) $Re=9229$ for $H/D_f = 0.6$

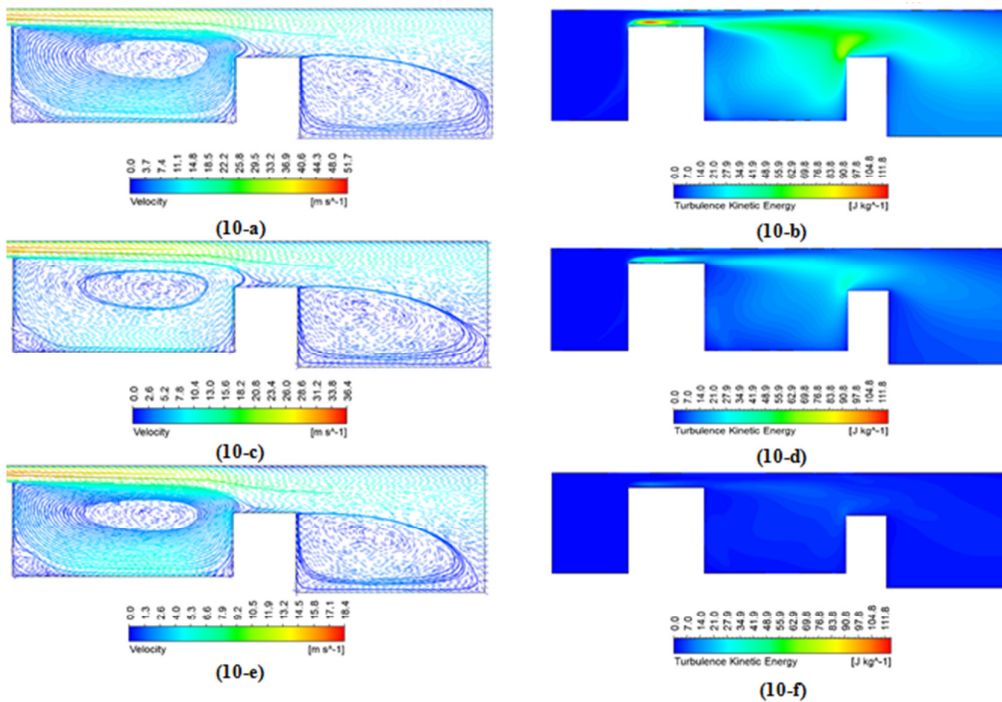


Fig. 10. Cavity flow structure at (10-a, b) $Re=27687$, (10-c, d) $Re=18458$, and (10-e, f) $Re=9229$ for $H/D_f = 1$

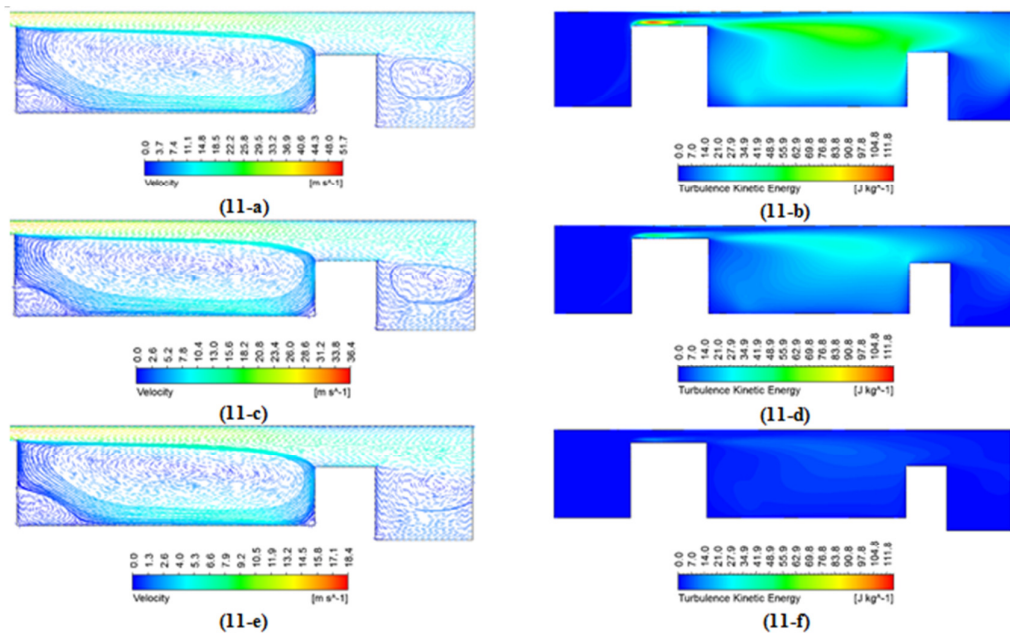


Fig. 11. Cavity flow structure at (11-a, b) $Re=27687$, (11-c, d) $Re=18458$, and (11-e, f) $Re=9229$ for $H/D_f = 1.4$

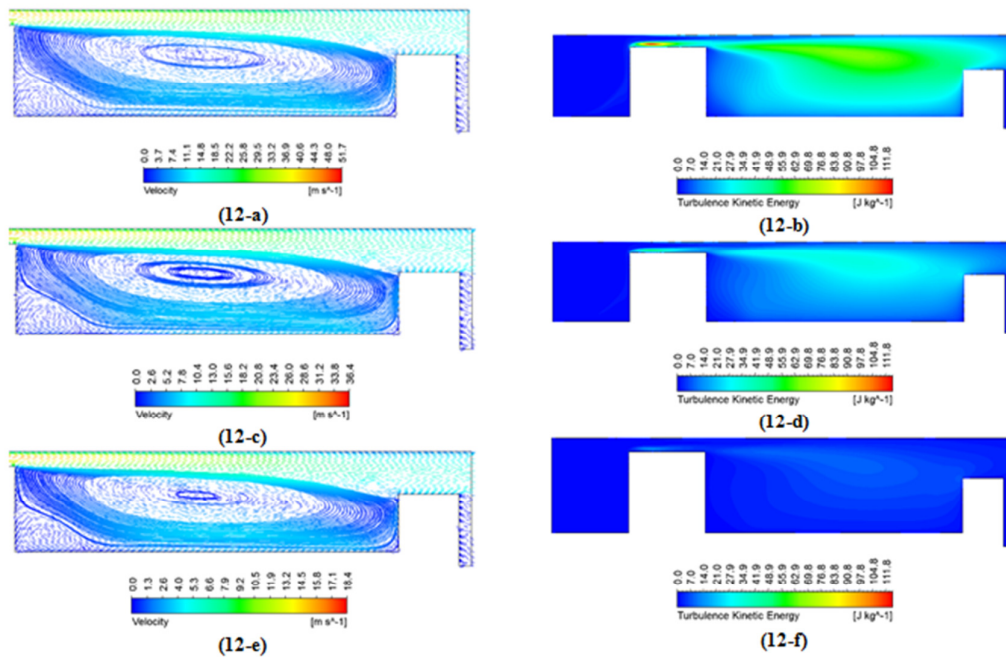


Fig. 12. Cavity flow structure at (12-a, b) $Re=27687$, (12-c, d) $Re=18458$, and (12-e, f) $Re=9229$ for $H/D_f = 1.6$

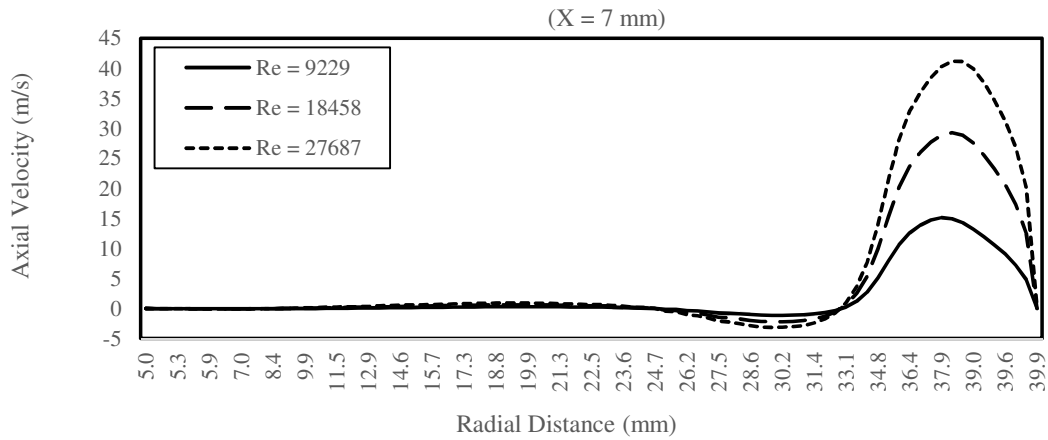


Fig. 13. Axial Velocity Distribution across vortex centreline – $H/D_f = 0.2$

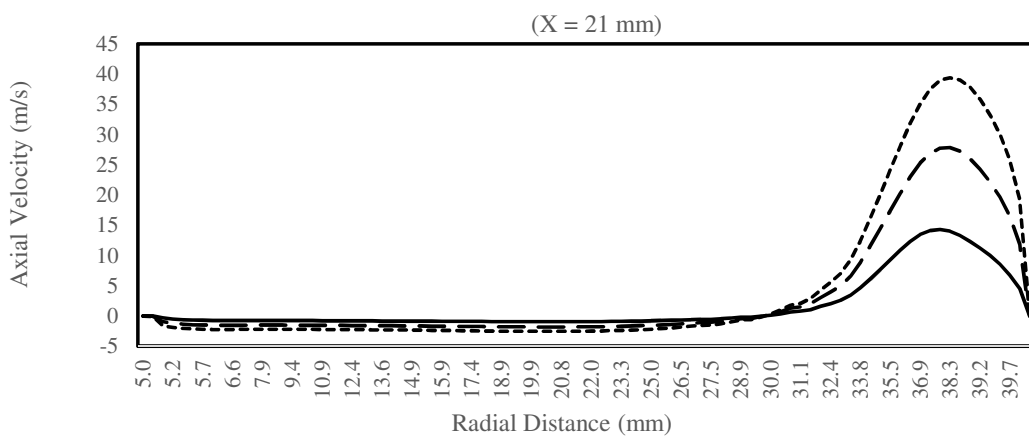


Fig. 14. Axial Velocity Distribution across vortex centreline – $H/D_f = 0.6$

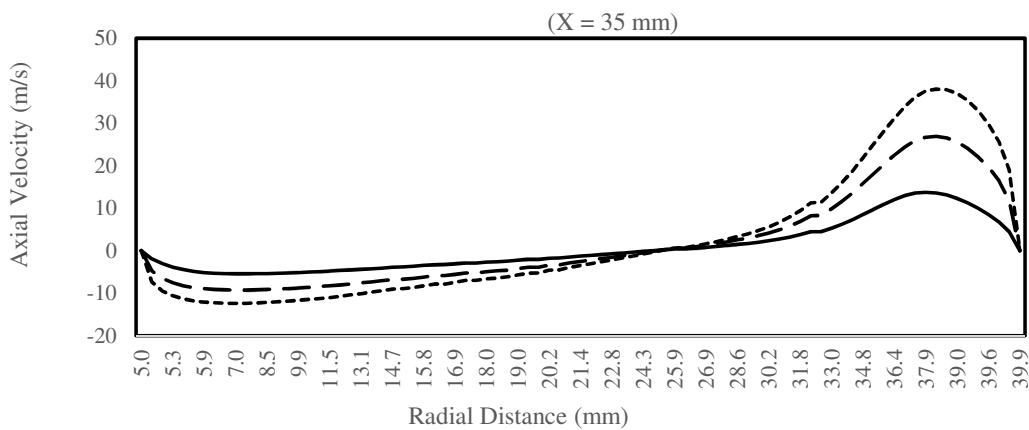


Fig. 15. Axial Velocity Distribution across vortex centreline – $H/D_f = 1$

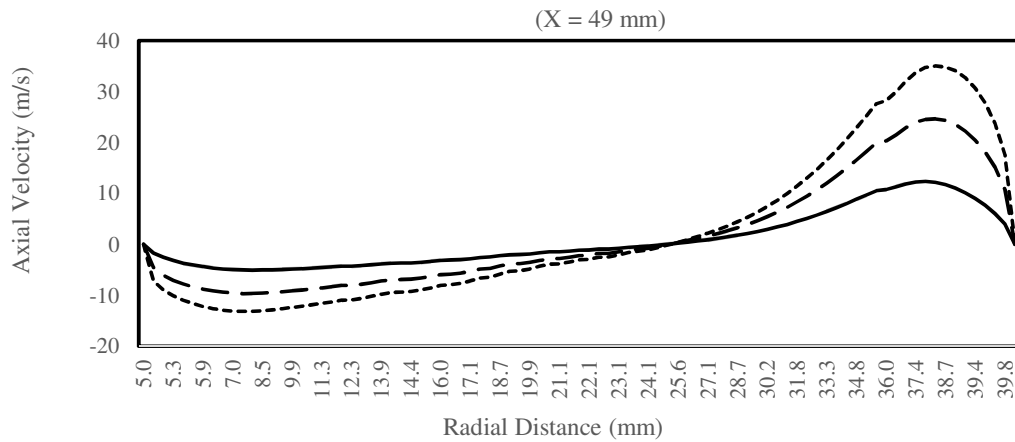


Fig. 16. Axial Velocity Distribution across vortex centreline – $H/D_f = 1.4$

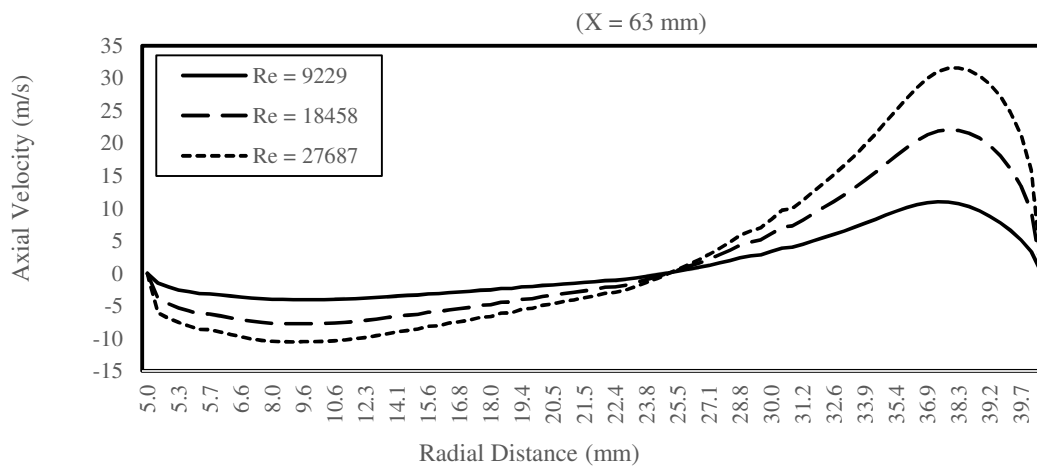


Fig. 17. Axial Velocity Distribution across vortex centreline – $H/D_f = 1.8$

4. Conclusion

Extensive numerical computations were conducted to: 1) Assess the ability of different RANS turbulence models to predict the flow physics of trapped vortices correctly, and 2) Study the effect of both main stream Reynolds number and cavity length on the cavity flow structure. This study was conducted to provide a ground base for future combustion analysis due to the high demonstrated potential of trapped vortex combustors in terms of low pressure drop and wide stability range. It was found that RSM turbulence model can correctly predict the flow structure inside the cavity for the whole range of cavity length and Reynolds numbers studied. Regarding pressure drop predictions, RSM was found to have the least prediction error percentage against experimental data with maximum value of 12.1% for all cases studied compared with 23.9 % demonstrated by the SST-KW which was the least accurate model. Increasing inlet flow Re by order of magnitude had no apparent effect on the main flow structure for the same cavity size. However, the 300 % Re increase from 9229 to 27687 has led to 10 times increase in turbulence levels and 3 times increase in recirculation zone strength which is good for mixing and flame stability, regarding combustion. Finally, multiple vortex structures, either behind the forebody for smaller cavity sizes of $H/D_f < 0.6$ or behind the afterbody for larger cavity sizes $H/D_f > 1$, were noticed to be the main reason behind increased pressure drop from 0.8 to 1.1%.

References

- [1] Ringleb, Friedrich O. "Separation control by trapped vortices." *Boundary Layer and Flow Control* 1 (1961): 265-294.
- [2] Mair, W. A. "The effect of a rear-mounted disc on the drag of a blunt-based body of revolution." *The Aeronautical Quarterly* 16, no. 4 (1965): 350-360.
- [3] Little, B. H., and R. R. Whipkey. "Locked vortex afterbodies." *Journal of Aircraft* 16, no. 5 (1979): 296-302.
- [4] Hsu, K-Y., L. P. Goss, and W. M. Roquemore. "Characteristics of a trapped-vortex combustor." *Journal of Propulsion and Power* 14, no. 1 (1998): 57-65.
- [5] Sidik, Nor Azwadi Che, and Siti Aisyah Razali. "Various speed ratios of two-sided lid-driven cavity flow using lattice Boltzmann method." *Journal of Advanced Research in Fluid Mechanics and Thermal Sciences* 1 (2014): 11-18.
- [6] Blunck, David, Dale Shouse, Craig Neuroth, Ryan Battelle, Amy Lynch, Balu Sekar, Joseph Zelina et al. "Experimental and computational studies of an Ultra-Compact Combustor." In *ASME Turbo Expo 2013: Turbine Technical Conference and Exposition*, pp. V01AT04A026-V01AT04A026. American Society of Mechanical Engineers, 2013.
- [7] Briones, Alejandro M., Balu Sekar, Dale T. Shouse, David L. Blunck, Hugh J. Thornburg, and Timothy J. Erdmann. "Reacting Flows in Ultra-Compact Combustors with Combined-Diffuser Flameholder." *Journal of Propulsion and Power* 31, no. 1 (2014): 238-252.
- [8] Briones, Alejandro, Hugh Thornburg, Balu Sekar, Craig Neuroth, and Dale Shouse. "Numerical-Experimental Research of Ultra Compact Combustors Containing Film and Effusion Cooling." In *51st AIAA Aerospace Sciences Meeting including the New Horizons Forum and Aerospace Exposition*, p. 1045. 2013.
- [9] Bucher, Jonathan, Ryan G. Edmonds, Robert C. Steele, Donald W. Kendrick, Blake C. Chenevert, and Philip C. Malte. "The development of a lean-premixed trapped vortex combustor." In *ASME Turbo Expo 2003, collocated with the 2003 International Joint Power Generation Conference*, pp. 207-213. American Society of Mechanical Engineers, 2003.
- [10] Burguburu, Joseph, Gilles Cabot, Bruno Renou, Abdelkrim Mourad Boukhalfa, and Michel Cazalens. "Flame stabilization by hot products gases recirculation in a Trapped Vortex Combustor." In *ASME Turbo Expo 2012: Turbine Technical Conference and Exposition*, pp. 319-328. American Society of Mechanical Engineers, 2012.
- [11] Hendricks, R. C., D. T. Shouse, W. M. Roquemore, D. L. Burrus, B. S. Duncan, R. C. Ryder, A. Brankovic, N-S. Liu, J. R. Gallagher, and J. A. Hendricks. "Experimental and computational study of trapped vortex combustor sector rig with high-speed diffuser flow." *International Journal of Rotating Machinery* 7, no. 6 (2001): 375-385.
- [12] Losurdo, Marco, Claudio Bruno, and Luigi Patignani. "Numerical Simulations of Trapped Vortex Combustors. Feasibility study of TVC integration in traditional GT combustion chambers." In *42nd AIAA/ASME/SAE/ASEE Joint Propulsion Conference & Exhibit*, p. 5140. 2006.
- [13] Patignani, L., M. Losurdo, and C. Bruno. "Numerical studies of the integration of a trapped vortex combustor into traditional combustion chambers." *International Flame Research Foundation Combustion Journal* 4 (2010).
- [14] WANG, Zhi-kai, Zhuo-xiong ZENG, L. I. Kai, and Yi-hua XU. "Effect of structure parameters of the flow guide vane on cold flow characteristics in trapped vortex combustor." *Journal of Hydrodynamics, Ser. B* 27, no. 5 (2015): 730-737.
- [15] Wu, Zejun, Yi Jin, Xiaomin He, Chong Xue, and Liang Hong. "Experimental and numerical studies on a trapped vortex combustor with different struts width." *Applied Thermal Engineering* 91 (2015): 91-104.
- [16] Jiang, Bo, Yi Jin, Dong Liu, Zejun Wu, Guoyu Ding, Zhixin Zhu, and Xiaomin He. "Effects of multi-orifice configurations of the quench plate on mixing characteristics of the quench zone in an RQL-TVC model." *Experimental Thermal and Fluid Science* 83 (2017): 57-68.
- [17] Katta, V., and W. Roquemore. "Numerical studies of trapped-vortex combustor." In *32nd Joint Propulsion Conference and Exhibit*, p. 2660. 1996.
- [18] Katta, Viswanath R., and W. M. Roquemore. "Numerical studies on trapped-vortex concepts for stable combustion." *Journal of engineering for gas turbines and power* 120, no. 1 (1998): 60-68.
- [19] Yasin, M.F.M., S. Cant, and M. Arqam. "Validation of a benchmark methanol flame using Open FOAM." *Journal of Advanced Research in Fluid Mechanics and Thermal Sciences* 28 (2016): 7-16.
- [20] Kumar, PK Ezhil, and D. P. Mishra. "Numerical investigation of the flow and flame structure in an axisymmetric trapped vortex combustor." *Fuel* 102 (2012): 78-84.
- [21] Versteeg, Henk Kaarle, and Weeratunge Malalasekera. *An introduction to computational fluid dynamics: the finite volume method*. Pearson Education, 2007.
- [22] J.O., H. Turbulence. . 1975. New York: McGraw-Hill Publishing Co.,.
- [23] Shih, Tsan-Hsing, William W. Liou, Aamir Shabbir, Zhigang Yang, and Jiang Zhu. "A new k- ϵ eddy viscosity model for high reynolds number turbulent flows." *Computers & Fluids* 24, no. 3 (1995): 227-238.

-
- [24] Menter, Florian R. "Two-equation eddy-viscosity turbulence models for engineering applications." *AIAA Journal* 32, no. 8 (1994): 1598-1605.
- [25] Launder, B. E., G. Jr Reece, and W. Rodi. "Progress in the development of a Reynolds-stress turbulence closure." *Journal of Fluid Mechanics* 68, no. 3 (1975): 537-566.
- [26] Jehad, D. G., G. A. Hashim, A. K. Zaroor, and CS Nor Azwadi. "Numerical Study of Turbulent Flow over Backward-Facing Step with Different Turbulence Models." *Journal of Advanced Research Design* 4, no. 1 (2015): 20-27.
- [27] M. K. Wong, L.C.S., C. S. Nor Azwadi, G. A. Hashim. "Numerical Study of Turbulent Flow in Pipe with Sudden Expansion." *Journal of Advanced Research in Fluid Mechanics and Thermal Sciences* 6 (2015): 34-48.